Structural phase transition in $Zn_{1.98}Mn_{0.02}P_2O_7$: EPR evidence for enhanced line broadening and large zero-field splitting parameter in high temperature phase

Santosh K. Gupta[a] and Ramakant Mahadeo Kadam
Radiochemistry Division, Bhabha Atomic Research Center, Trombay, Mumbai-400085, India

Pradeep Samui
Product Development Division, Bhabha Atomic Research Center, Trombay, Mumbai-400085, India

Krishnan Kesavaiyer
Fuel Chemistry Division, Bhabha Atomic Research Center, Trombay, Mumbai-400085, India

Venkataraman Natarajan and Shrikant Vasant Godbole
Radiochemistry Division, Bhabha Atomic Research Center, Trombay, Mumbai-400085, India

(Received 24 June 2013; accepted 17 October 2013)

$Zn_{1.98}Mn_{0.02}P_2O_7$ was synthesized by the wet chemical route. The purity of the phase and the oxidation state of manganese ion were investigated by x-ray diffraction (XRD) and electron paramagnetic resonance (EPR). Structural phase transition in α-$Zn_2P_2O_7$ was investigated by high-temperature XRD (HTXRD), differential scanning calorimetry (DSC), and EPR studies. There is a distinct signature of phase transitions between 390 and 400 K in our powder sample by EPR and HTXRD. There was a sharp reduction in the volume of unit cell, while going from alpha to beta phase; with discontinuity in 405 K, which confirmed the transition to be of first order. Similarly, the effect of temperature on zero-field splitting parameter (D) also showed that there is a sudden jump (discontinuity) in the value at around 400 K (phase transition temperature) confirming the transition to be of first order. DSC studies corroborated these findings.

I. INTRODUCTION

Phosphate-based systems offer a range of compositional and structural possibilities (Ultra, Meta, Pyro, and Ortho) that facilitate tailoring chemical and physical properties of interest for specific applications. They are capable of forming polymers having a series of rings or chains by P–O bonds and have potential applications as technological materials due to their good thermal and chemical stabilization.[1] They offer better homogeneity, chemical and thermal stability with lower sintering temperatures.[2–4]

The structures of pyro- and metaphosphate systems are well known. Metal ion polyhedra clusters by sharing corners, forming a cation subnetwork that links the separate phosphate anions. Special interest in pyrophosphate arises from the unique spectroscopic behavior of the metal cation polyhedra with well-defined and low symmetry coordination.[5] Pure and doped pyrophosphates are technologically important because of their luminescent, dielectric, semiconductor, catalytic, magnetic, fluorescent and ion-exchange properties. Therefore, the synthesis of pyrophosphates is an active field of research for many investigators. Moreover, pyrophosphate $A_2P_2O_7$ (A = Ca, Sr, Ba, Mg, Zn, Mn) have been reported to possess good microwave dielectric properties as well as relatively low sintering temperature.[6] Among them, thortveitite-type pyrophosphate α-$Zn_2P_2O_7$ exhibits rather low sintering temperature (875 °C) and is a very promising low temperature cofired ceramic material.[7] The size of the A^{n+} and $B^{(7-n)+}$ cations plays an important role in determining the type of the crystalline structure. When the ionic radius of B is greater than 0.5 Å, the observed structure types are pyrochlore or weberite, and if the ionic radius of B is less than 0.5 Å, the observed structure types are dichromate or thortveitite.[8] These compounds have been obtained with phosphorus, vanadium, silicon, and chromium in their highest oxidation state. The crystal structure can therefore be formulated as ionic with A as the cation and B_2O_7 as the anion. B_2O_7 consists of two BO_4 tetrahedra sharing an oxygen atom with a B–O–B angle of approximately 130°. The crystal structures of the diphosphates $A_2P_2O_7$, where A is a divalent cation, have been widely studied. $A_2P_2O_7$ (A = Ca, Sr, Ba, Mg, Zn) is a large family of pyrophosphate compounds, which have been found to crystallize in two structural types that can be predicted from the ionic radius of A cation. When radius of A^{2+} is smaller than 0.97 Å (A = Mg, Mn, Fe, Co, Ni, Cu, Zn), $A_2P_2O_7$ is of the thortveitite structure, in which $[P_2O_7]^{4-}$ groups are in the staggered configuration, and when the radius of A^{2+} is

[a]Address all correspondence to this author.
e-mail: santufrnd@gmail.com
DOI: 10.1557/jmr.2013.325

 © Materials Research Society 2013

https://doi.org/10.1557/jmr.2013.325 Published online by Cambridge University Press

larger than 0.97 Å (A = K, Ca, Sr, Rb, Ba, Pb, Cd), $A_2P_2O_7$ is of the dichromate structure, in which $[P_2O_7]^{4-}$ groups are in eclipsed configuration.[8] Therefore, $Zn_2P_2O_7$ is having thortveitite structure, in which $[P_2O_7]^{4-}$ groups are in the staggered configuration. Two polymorphic transformations of zinc pyrophosphate have been known to exist. They are α and β modifications connected with each other by reversible transformation at 405 K. The high temperature β-modification exists at the temperature of congruent melting, 1288 K.[9]

Zinc pyrophosphate, $Zn_2P_2O_7$, is one of the families which are isostructural in their high temperature (β) phase. The low temperature (α) phase falls into three groups, each a multipartite, defined by Lefkowitz et al.,[10] of its parent phase. These groups consist of $Cu_2P_2O_7$, which is bipartite along *c*-axes; $Mg_2P_2O_7$, $Ni_2P_2O_7$, and $Co_2P_2O_7$, which are bipartite along both *c* and *a* axes; and $Zn_2P_2O_7$, which is bipartite along *c* axis and tripartite along *a* axis.[11] The length of *b*-axes and the β-angles remains substantially the same through the transitions. In terms of the gross structure, α-$Zn_2P_2O_7$ is the most complex of the series.

The structure of thortveitite β-$Zn_2P_2O_7$ is characterized by having a staggered (noneclipsed) conformation of $[P_2O_7]^{4-}$ anions, with almost linear P–O–P bonds and an irregular octahedral coordination for Zn^{2+}. Endothermic reversible transitions have been reported for $Zn_2P_2O_7$ at 405 K[12] and for $Mg_2P_2O_7$ at 341 K.[13] $Cu_2P_2O_7$ has a phase transition at 345 K, whereas in contrast no phase transition has been found in $Mn_2P_2O_7$. Phase transition in single crystals of $Zn_2P_2O_7$ has been investigated by electron paramagnetic resonance (EPR) using Mn^{2+} as a probe.[14] We could detect the phase transition in powder sample also. EPR[15–18] and XRD[19–21] as techniques have been extensively used to understand the phase transition in various inorganic systems.

EPR experiments are used to get information about the oxidation state, the site occupancy, and the coordination sphere of the transition metal ions doped in different inorganic matrices.[22,23] It is also useful in getting information about the local site symmetry around the paramagnetic ion and in quantifying the number of unpaired spins of different paramagnetic ions.

Mn^{2+} being EPR sensitive is chosen as a probe ion to investigate structural phase transformation in powder zinc pyrophosphate because the isostructural relationship of the high-temperature forms permits a definite assignment of the Mn^{2+} site in the structure and more importantly because the relatively high sensitivity of the electron spin resonance (ESR) spectra to the Mn^{2+} environment might permit a detailed study of the various phase transitions. Divalent Cu and Mn have previously been studied in $Zn_2P_2O_7$ by ESR.[14] This study confirmed the reported first-order phase transition at 405 K.[12] In the present work, zinc pyrophosphate (both pure and doped sample) has been synthesized by the wet chemical route and characterized by x-ray diffraction (XRD), differential scanning calorimetry (DSC), and EPR. Moreover, structural phase transformation was investigated by high-temperature EPR. The same was corroborated with high-temperature XRD (HTXRD) and DSC.

II. EXPERIMENTAL

A. Sample preparation

Zinc hydrogen phosphate was precipitated from zinc nitrate solution containing Mn^{2+} (2 mol%) by adding $(NH_4)_2HPO_4$. The pH of the solution was adjusted to be around 7–8. Analytical grade zinc nitrate, $(NH_4)_2HPO_4$, and very pure $MnCO_3$ (99.999%) were used for the preparation. The precipitate was filtered and dried with alcohol. Later, it was ground thoroughly and heated at 950 °C for 3–4 h in air.

B. Instrumentation

The phase purity of the prepared phosphors was confirmed by XRD. The measurements carried out on a STOE x-ray diffractometer (Germany) equipped with a Ni filter, a scintillation counter, and a graphite monochromator. The diffraction patterns were obtained using monochromatic Cu K_α radiation (λ = 1.5406 Å) keeping the scan rate at 1 s/step in the scattering angle range (2θ) of 10–60°. The $K\alpha_2$ reflections were removed by a stripping procedure to obtain accurate lattice constants and grain sizes. The EPR spectra were recorded on a Bruker ESP-300 spectrometer (Switzerland) operating at X-band frequency (9.5 GHz) equipped with 100-kHz field modulation and phase sensitive detection to obtain the first derivative signal. Diphenyl picrylhydrazyl (DPPH) was used for the calibration of *g* values of paramagnetic species. The EPR parameters have been precisely determined from the calculated spectra, obtained using BRUKER SIMFONIA program. The simulations were carried out assuming mixed line shape (Lorentzian/Gaussian = 0.5) with a peak-to-peak line width of 0.01 T. HTXRD studies of $Zn_2P_2O_7$ were carried out using a STOE diffractometer fitted with HDK-2.4 high temperature attachment. About 10 mg of the finely ground sample was mounted on a Pt-Rh strip, which acts as both a sample holder and a heater for HTXRD studies. Pt/Pt-13% Rh thermocouple spot welded at the bottom of the sample holder was used for the measurement of temperature. The temperature calibration and alignment of the diffractometer was checked by measuring the thermal expansion coefficient of MgO. The sample was heated under vacuum (~10–5 mbar) at the rate of 15 K/min to the predetermined temperature and held for 30 min prior to data collection. The XRD pattern was recorded in the range of $10 \leq 2\theta \leq 50°$ from room temperature to 1273 K.

Determination of phase transitions of samples was carried out using a heat flux type differential scanning calorimeter (DSC-131, SETARAM Instrumentation, France). Temperature calibration for the calorimeter was done using

https://doi.org/10.1557/jmr.2013.325 Published online by Cambridge University Press

the phase transition temperatures of NIST reference materials (indium: T_{fus} = 429.748 K; tin: T_{fus} = 505.078 K; lead: T_{fus} = 600.600 K; mercury: T_{fus} = 234.316 K; potassium nitrate: T_{trs} = 400.850 K; and silver sulfate; T_{trs} = 703.150 K). Heat calibration of the calorimeter was carried out using the transition heats of the above-mentioned materials. For determination of the phase transition temperature, in the first run, two empty aluminum crucibles of identical masses (10^{-4} dm^3 capacity) covered with lid were kept in the sample and reference cells, and the heat flow versus temperature were measured in the temperature range of 300–473 K at a heating rate of 2 K/min with high purity argon as the carrier gas with a flow rate of 2 dm^3/h. In the second run, the heat flow versus temperature were measured by loading the sample in the powder form (~200 mg) in the sample cell while the reference cell was left empty.

III. RESULTS AND DISCUSSION

A. Characterization: XRD and EPR spectroscopy

The XRD patterns of the pure and Mn-doped zinc pyrophosphate sample are shown in Fig. 1, from which it can be seen that all the diffraction peaks of both samples can be indexed to the monoclinic phase of α-$Zn_2P_2O_7$ (ICDD card No. 08–0238). This indicates that Mn^{2+} occupies the zinc lattice position and has not distorted the crystal structure. Since no impurity peaks are observed, it is feasible to suggest that both samples exist in single phase, i.e., α-$Zn_2P_2O_7$. The crystallographic data of α-$Zn_2P_2O_7$ lattice is listed in Table I. The XRD data of the relatively intense peak ($I/I_0 > 10$) were indexed on a monoclinic system with space group $I2/c$ having cell parameters a = 19.59 ± 0.01 Å, b = 8.282 ± 0.01 Å, and c = 9.103 ± 0.01 Å and β = 100.45 ± 0.2° as represented in Table II. These parameters were obtained

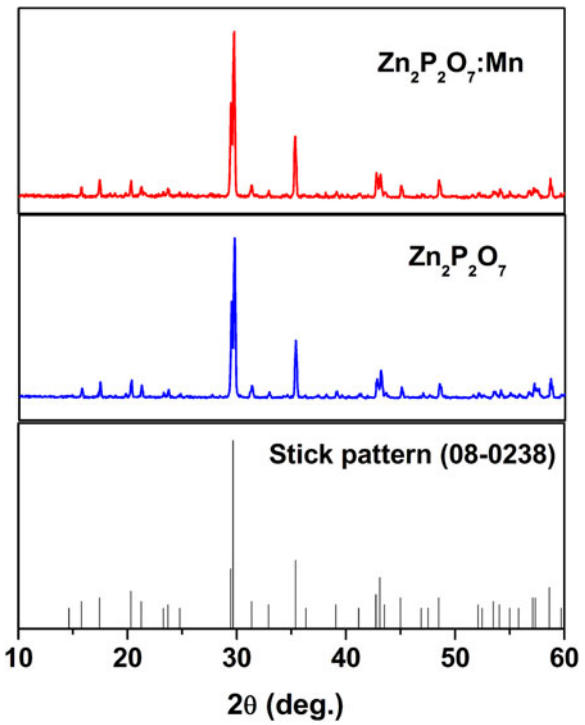


FIG. 1. XRD pattern of the undoped $Zn_2P_2O_7$ and 2 mol% Mn^{2+}-doped $Zn_2P_2O_7$ annealed at 950 °C (as prepared sample).

TABLE I. Crystallography data for α-$Zn_2P_2O_7$ lattice.

Z	12
Crystal system	Monoclinic
Lattice	End centered
Space group	I2/c
Formula weight	304.70
Density	4.24 g/cm^3
Lattice parameter	
a (Å)	19.59 ± 0.01
b (Å)	8.282 ± 0.01
c (Å)	9.103 ± 0.01
β	100.45 ± 0.2°

TABLE II. XRD data of α-$Zn_2P_2O_7$ (λ = 0.15406 nm) annealed at 950 °C.

2θ values	d value (Å)	I/I_0 (%)	h k l
29.454	3.0300	25	$\bar{1}$ 0 3
29.655	3.0100	100	$\bar{2}$ 0 3
35.379	2.5350	36	3 3 0
42.759	2.1130	14	$\bar{4}$ 1 4
43.101	2.0970	29	$\bar{5}$ 3 2
44.966	2.0130	12	$\bar{6}$ 0 4
48.512	1.8750	13	$\bar{7}$ 3 2
53.512	1.7110	11	7 3 2
57.128	1.6110	15	9 0 3
57.322	1.6060	15	$\bar{12}$ 0 2
58.640	1.5730	27	6 4 2

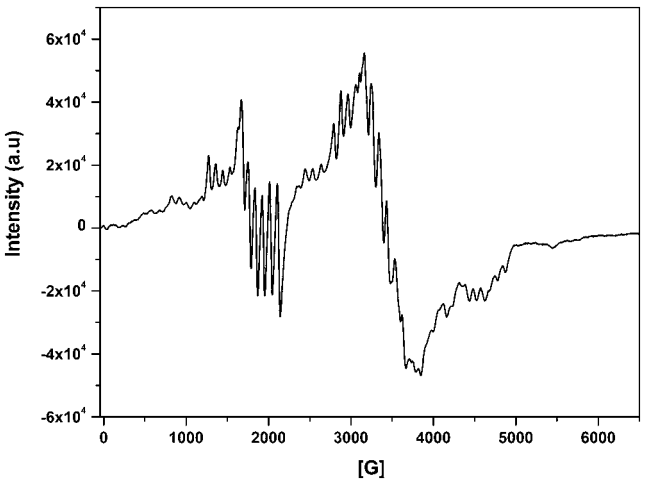


FIG. 2. Room temperature EPR spectra of $Zn_2P_2O_7$:Mn.

https://doi.org/10.1557/jmr.2013.325 Published online by Cambridge University Press

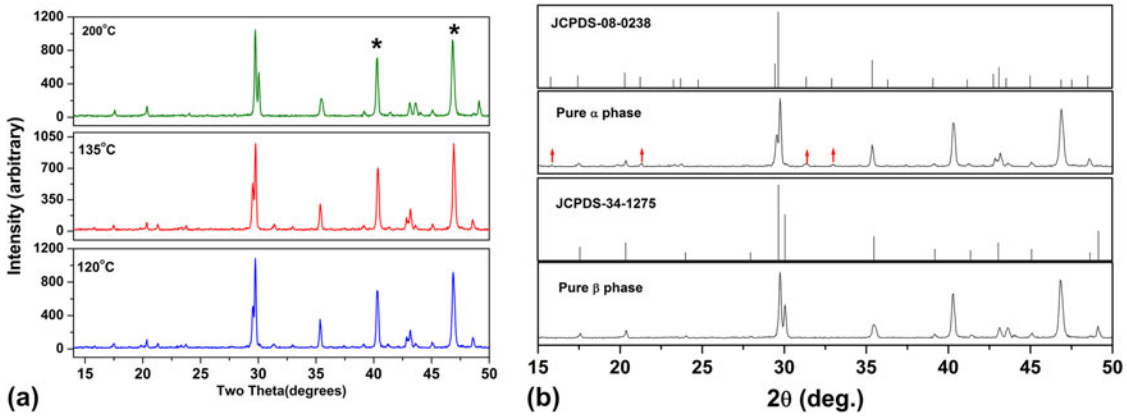


FIG. 3. (a): XRD pattern of 2 mol% Mn^{2+} in $Zn_2P_2O_7$ at various temperatures (b) XRD pattern α and β phase and their standard pattern of 2 mol% Mn^{2+} in $Zn_2P_2O_7$. Arrows indicate missing reflections in β-phase.

by Rietveld refinement of α-$Zn_2P_2O_7$ (ICDD card No. 08–0238) having a space group *I*2/*c*.

Figure 2 shows the room temperature EPR spectrum of Mn^{2+}-doped $Zn_2P_2O_7$. EPR can differentiate between Mn^{2+} and Mn^{4+} due to the difference in the number of fine transitions and the *g* values (Mn^{4+}, $S = 3/2$, three fine transitions and $g < 2.00$; Mn^{2+} $S = 5/2$, five fine transitions and $g = 2.00$). However, Mn^{3+} (nonKramer ion with $S = 2$), though paramagnetic, may not be detected due to the possibility of the ground state being singlet and zero-field splitting being large.

The ground state of Mn^{2+} with d^5 configuration is unique among d^n configurations in that there is only one state with maximum spin multiplicity ($^6S_{5/2}$). In the case of d^5 transition metal ions, the axial distortion of octahedral symmetry gives rise to three Kramer's doublets ±5/2, ±3/2, and ±1/2.[24] Application of a Zeeman field lifts the spin degeneracy of the Kramer's doublets. As the crystal field splitting is normally much greater than the Zeeman field, the resonance observed is due to transition within the Zeeman field split of Kramer's doublets. The ESR spectrum of Mn^{2+} in undiluted samples exhibits a broad resonance of $g \sim 2.0$. In diluted samples, it shows six allowed transitions ($\Delta Ms = \pm 1$ and ± 0) due to the nuclear spin of ^{55}Mn ($I = 5/2$) or 30 lines due to finite zero-field splitting of Kramer's doublets and nuclear spin interaction.

TABLE III. Allotropic forms and crystallographic data of $Zn_2P_2O_7$.

A	Allotropic form	Space group	Coordination group	P–O–P angle (deg)	P–O bond length (Å)
Zn	α	*I*2/*c*	5,6	139 and 148	Mean P–O = 1.557
					$P–O_{br}$ = 1.569
	β	*C*2/*m*	Only 6	180 (linear)	$P–O_{nbr}$ = 1.553

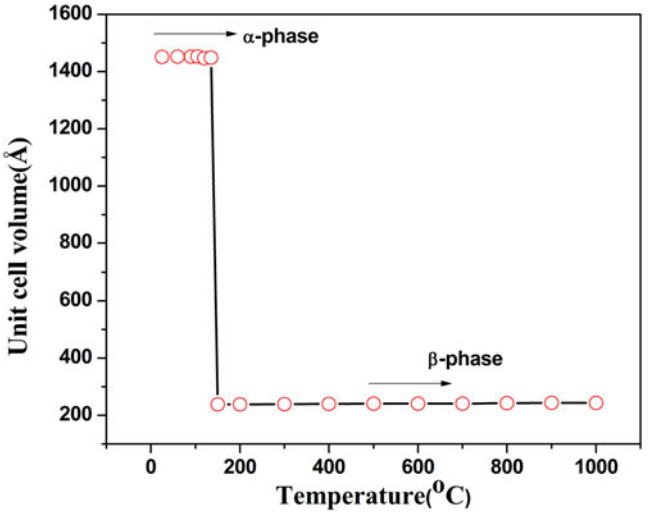


FIG. 4. The temperature variation of the unit cell volume of 2 mol% Mn^{2+} in $Zn_2P_2O_7$. Error bars are smaller than symbols.

B. Structural phase transition: HTXRD, DSC, and EPR

HTXRD pattern is shown in Fig. 3(a). There is pure α-phase at 120 °C; phase transformation takes place at 405 K, which is having mixed features of α and β, but at 473 K, pure β-phase is seen. Individual XRD patterns of α and β phase and their standard pattern are shown in Fig. 3(b). Crystallographic data of zinc pyrophosphate is mentioned in Table III. Lattice parameter obtained for β phase is $a = 6.61 \pm 0.01$ Å, $b = 8.29 \pm 0.01$ Å, and $c = 4.51 \pm 0.01$ Å and $\beta = 105.4 \pm 0.2°$.

Although structurally both are same, i.e., monoclinic, they crystallize in different space groups. α-phase has lower symmetry *I*2/*c* space group, whereas β is having more symmetric *C*2/*m* space group. From the XRD pattern, it can be seen that reflections at 2θ values of 16.414, 21.344, 30.0487, and 31.972 completely disappears in more symmetric β-phase. In the β-phase, the four cations in the unit cell lie on the twofold axes and are symmetry related by

https://doi.org/10.1557/jmr.2013.325 Published online by Cambridge University Press

the centering operation (1/2, 1/2, 0) and by the mirror plane. The variation in the unit cell volume from 298 to 1023 K is shown in Fig. 4. On going from α to β, the phase length of *a*- and *c*-axis is reduced by a factor of 1/3 and 1/2 as is observed using HTXRD. This is the reason for volume reduction in the unit cell, while going from alpha to beta phase. There is sudden discontinuity in volume at 405 K which shows that transition is of first order. This result has also been corroborated with differential scanning calorimetry (DSC). Around 405 K, zinc pyrophosphate undergoes a reversible, first order isostructural transition, the phenomenon being supported by the DSC data (Fig. 5).

Crystal structures of zinc pyrophosphate (both α and β) are shown in Fig. 6. These structures were drawn using the VESTA visualization program.[25] In both these phases $[P_2O_7]^{4-}$ anions assume staggered confirmation as shown in Fig. 7.

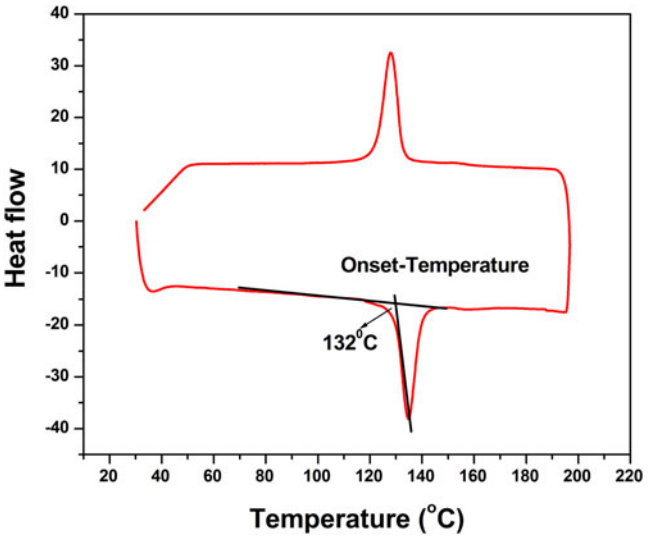


FIG. 5. DSC studies of Mn-doped $Zn_2P_2O_7$.

The structure of the α-phase is characterized by a sequence of layers. A layer like that found in α-$Cu_2P_2O_7$ is followed by two layers like those found in α-$Mg_2P_2O_7$.[11] The former layers have anions lying on 2-fold axes, and the cations are coordinated to five oxygen atoms; in the next two layers, half of the cations are five coordinates and another half is six coordinated, and the anions in these layers show only approximate twofold axes. All the anions show nonlinear P–O–P bonds.

The crystal structure of β-phase is identical with that of $Mn_2P_2O_7$.[26] In β-phase, the structure is described by alternate anion and cation layers stacked along the *c* direction and observed at $z = 0$ and $z = 1/2$, respectively. The asymmetric unit contains a unique Zn^{2+} cation. The short distance between cations along the *c* direction is about 4.51 Å. In the cationic layers, Zn^{2+} is found on 2-fold axes in irregular 6-fold coordination,[27] i.e., they are not at the center of the oxygen atom environment and displaced by about 0.3 Å from a line joining O3 to its mate generated by the 2-fold axis.

The major component of these distortions arises from a rotation of the O3–O3 edge from its ideal position by 30° about the 2-fold axis. Such a distortion arises from the constraints placed upon the positions of the oxygen atoms by the requirements of its bonding to the phosphorus atom. Detailed crystallographic data of both these two phases are mentioned in Table III.

Temperature-dependent EPR investigation of Mn in $Zn_2P_2O_7$ is shown in Fig. 8. Robertson and Calvo[11] have reported EPR evidence for phase transition in single crystals

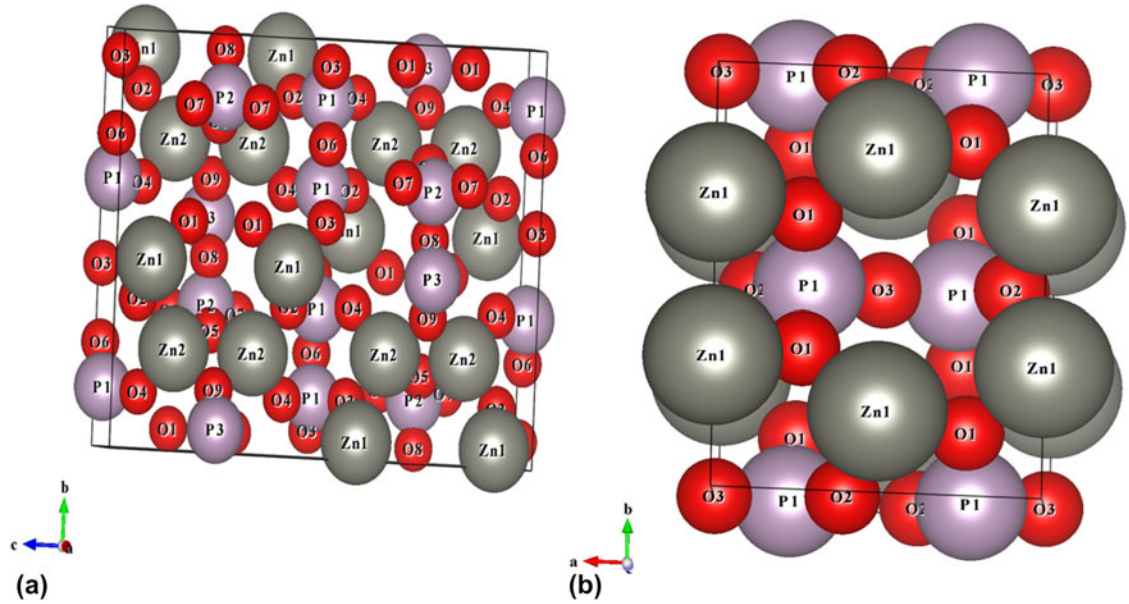


FIG. 6. Crystal structure of (a) α-$Zn_2P_2O_7$ and (b) β-$Zn_2P_2O_7$.

https://doi.org/10.1557/jmr.2013.325 Published online by Cambridge University Press

of $Zn_2P_2O_7$ using Mn^{2+} as an EPR probe. Their studies have showed that α-$Zn_2P_2O_7$, the stable phase at room temperature, undergoes a first-order phase transition at 405 K and an inhomogeneous second-order transformation between 405 and 428 K. We could identify the phase transitions at 132 °C in our powder sample, but second-order phase transition is difficult to identify in the powder sample, although some kink at 428 K is obtained in DSC studies (Fig. 5), discussed earlier.

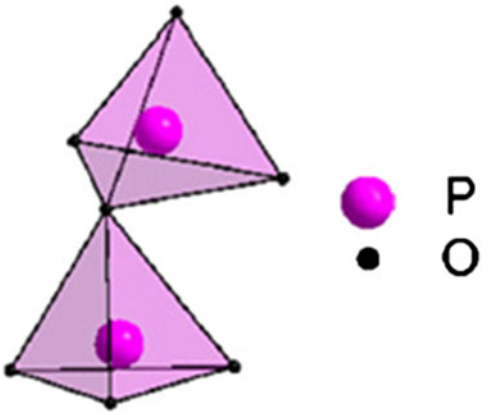


FIG. 7. The connection between two $[PO_4]$ tetrahedra in the $[P_2O_7]$ group showing a staggered configuration.

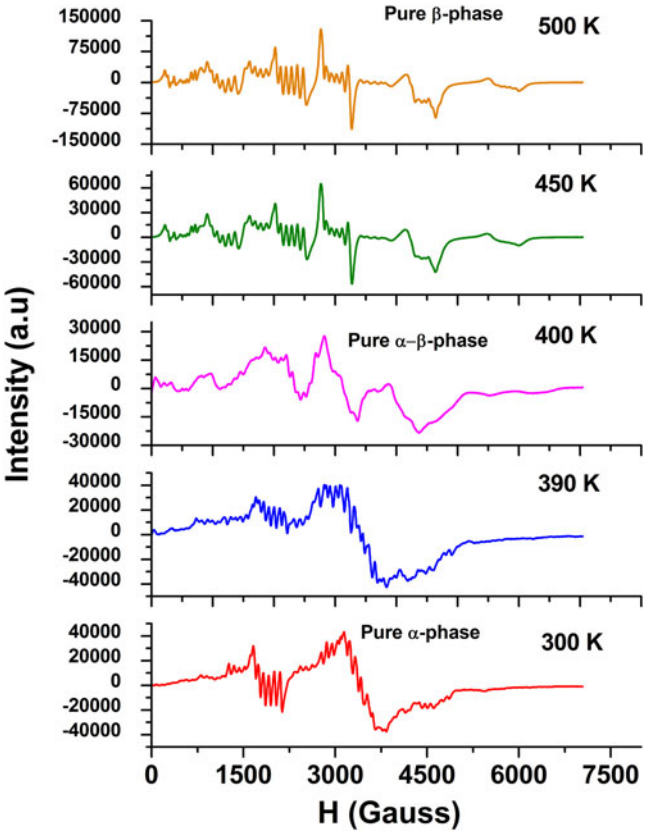


FIG. 8. EPR spectra of 2 mol% Mn^{2+} in $Zn_2P_2O_7$ at various temperatures.

It can be seen from the EPR pattern (Fig. 8) that spectra changes drastically going from 390 to 400 K. Highly resolved hyperfine sextet of Mn^{2+} can be seen till 390 K, whereas at 400 K, the hyperfine splitting completely disappears and the spectrum merges to a broad signal. Zero-field splitting parameter (D) was evaluated for Mn^{2+} from room temperature to 500 K (Fig. 9). It was observed that there is a sudden jump (discontinuity) in the value at 400 K (phase transition temperature) confirming the transition to be of first order.

The D value for Mn^{2+} in the β phase (1380 G) is unusually large. It is tempting to suggest that this large D value is related to the highly irregular cation environment. The D values in the intermediate temperature region, however, show very large changes from their high-temperature value despite an apparently small change in the electron density distribution of the crystal. These observations could be consistent only if D depends on a higher power of a component of the crystalline field. The enhanced line broadening in β-phase could result from a residual short range ordering near the transition temperature, which yields a small spread in the crystalline field. The fact that orthorhombic distortion term (E) is small in β-phase and a large change in D across the transition temperature suggests that the structural change involves primarily distortions along Zn–O3 bond. Since the bond between the central oxygen atom and adjacent phosphorous atom of the $[P_2O_7]^{4-}$ lies along the z-direction in the β-phase, it might be suggested that the mechanism for the change in structure involves primarily either a small change in length of these P–O bonds or a contraction of the P–O–P bond angle.

As evident by HTXRD and structural studies [Fig. 6(a)], in α-phase, there are two types of zinc ions: asymmetric 5-coordinated Zn^{2+} and relatively symmetric 6-coordinated

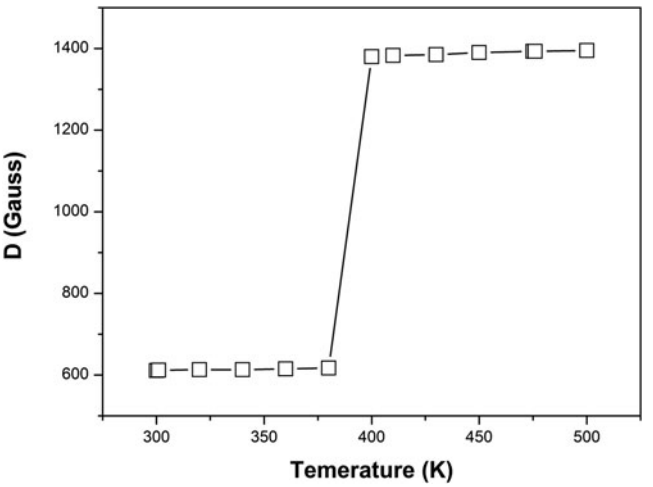


FIG. 9. The temperature variation of the zero-field splitting parameter for $Zn_2P_2O_7$:Mn^{2+}.

https://doi.org/10.1557/jmr.2013.325 Published online by Cambridge University Press

Zn^{2+} (Zn1 and Zn2). In the case of β-phase, only asymmetric 5-coordinated zinc exists (Zn1) as can be seen from Fig. 6(b).

Main changes in the EPR pattern from α to β phase are enhanced line broadening and unusual large zero-field splitting parameter. This can be correlated with the presence of distorted octahedra of oxygen around Zn^{2+} ion in β-phase. The phase transformation then requires that the five-fold coordinated sites of α phase form a sixth bond with oxygen atoms. This requires that oxygen atoms move from an average cation-oxygen distance of 3.2 Å to the "normal" bond distance of 2.15 Å found in β-$Zn_2P_2O_7$.

IV. CONCLUSIONS

Metal polyphosphates show a great variety of compositions, crystal structures, and properties. Nowadays, they have become an important constituent class of compounds for exploring new functional materials. Understanding their thermal and phase stability is very important for application in sensors, solid-state laser materials, piezoelectric, luminescence, ceramics, catalysis, adsorption, ionic conductors, and magnetic materials. We could identify the phase transitions between 390 and 400 K in our powder sample by EPR and HTXRD. DSC confirmed that the transition is reversible and is of 1st order. HTXRD has shown that the length of *a*-axis is tripled and *c*-axis is doubled in α-phase as compared to β-phase. This is the reason for volume reduction in the unit cell, while going from α to β phase. There is sudden discontinuity in volume at 405 K, which shows that the transition is of first order. The effect of temperature on zero-field splitting parameter was also studied, and there is a sudden jump (discontinuity) in the value at 400 K (phase transition temperature) confirming the transition to be of first order. The *D* value for Mn^{2+} in the β phase (1380 G) is unusually large, which is related to its highly irregular cation environment.

REFERENCES

1. L.H. Brixner: New x-ray phosphor. *Mater. Chem. Phys.* **16**, 253 (1987).
2. M. Zhao, L. Li, J. Zheng, L. Yang, and G. Li: Is $BiPO_4$ a better luminescent host? Case study on doping and annealing effects. *Inorg. Chem.* **52**, 807 (2013).
3. B.S. Naidu, B. Vishwanadh, V. Sudarsan, and R. Vatsa: BiPO4: A better host for doping lanthanide ions. *Dalton Trans.* **41**, 3194 (2012).
4. E. Song, W. Zhao, G. Zhou, X. Dou, H. Ming, and C. Yi: White light emitting from single phased $K_2Ca_{1-x-y}P_2O_7$: xEu^{2+}, yMn^{2+} phosphors under UV excitation. *Curr. Appl. Phys.* **11**, 1374–1378 (2012).
5. D.E. Day, Z. Wu, C.S. Ray, and P. Hrma: Chemically durable iron phosphate glass waste forms. *J. Non-Cryst. Solids* **241** 1 (1998).
6. G.K. Marasinghe, M. Karabulut, C.S. Ray, D.E. Day, D.K. Shuh, P.G. Allen, M.L. Saboungi, M. Grimsditch, and D. Haefner: Properties and structure of vitrified iron phosphate nuclear waste forms. *J. Non-Cryst. Solids* **263–264**, 146 (2000).
7. M. Karabulut, G.K. Marasinghe, C.S. Ray, D.E. Day, G.D. Waddill, C.H. Booth, P.G. Allen, J.J. Bucher, D.L. Caulder, and D.K. Shuh: An investigation of the local iron environment in iron phosphate glasses having different Fe (II) concentrations. *J. Non-Cryst. Solids* **306**, 182 (2002).
8. A. Boukhari: Diphosphate structures related to the dichromate or thortveitite type. *J. Alloys Compd.* **188**, 14 (1992).
9. I.D. Brown and C. Calvo: The crystal chemistry of large cation dichromates, pyrophosphates, and related compounds with stoichiometry $X_2Y_2O_7$. *J. Solid State Chem.* **1**, 173 (1970).
10. I. Lefkowitz, K. Lukaszewez, and H.D. Megaw: The high-temperature phases of sodium niobate and the nature of transitions in pseudosymmetric structures. *Acta Cryst.* **20**, 670 (1966).
11. B.E. Robertson and C. Calvo: Crystal structure of α-$Zn_2P_2O_7$. *J. Solid State Chem.* **1**, 120 (1970).
12. F.L. Katnack and F.A. Hummel: Phase equilibria in the system ZnO-P_2O_5. *J. Electrochem. Soc.* **105**, 125 (1958).
13. R. Roy, E.T. Middleswarth, and F.A. Hummel: Mineralogy and thermal behavior of phosphates I. Magnesium pyrophosphate. *Am. Mineral.* **33**, 458 (1948).
14. J.G. Chambers, W.R. Datars, and C. Calvo: ESR study of the crystallographic phases in $Zn_2P_2O_7$:Mn and $Zn_2P_2O_7$:Cu. *J. Chem. Phys.* **41**, 806 (1964).
15. M. Labrinia, I. Saadounea, A. Almaggoussib, J. Elhaskouric, and P. Amoros: The $Li_yNi_{0.2}Mn_{0.2}Co_{0.6}O_2$ electrode materials: A structural and magnetic study. *Mater. Res. Bull.* **47**, 1004 (2012).
16. J. Orive, R. Balda, J. Fernandez, L. Lezama, and M.I. Arriortua: Low temperature red luminescence of a fluorinated Mn-doped zinc selenite. *Dalton Trans.* **42**, 12481 (2013).
17. V.N. Voronov and E.A. Petrakovskaya: EPR investigation of local paramagnetic centers in perovskite-like crystals. *Phys. Solid State* **55**, 730 (2013).
18. M.L. Falin, K.I. Gerasimov, V.A. Latypov, A.M. Leushin, and N.M. Khaidukov: EPR and optical spectroscopy of structural phase transition in an Rb_2NaYF_6 crystal. *Phys. Rev. B* **87**, 115145 (2013).
19. J. Zhang, S. Yan, S. Zhao, Q. Xu, and C. Li: Photocatalytic activity for H_2 evolution of TiO_2 with tuned surface crystalline phase. *Appl. Surf. Sci.* **280**, 304 (2013).
20. A.A. Hubaud, D.J. Schroeder, B. Key, B.J. Ingram, F. Dogan, and J.T. Vaughey: Low temperature stabilization of cubic $(Li_{7-x}Al_{x/3})La_3Zr_2O_{12}$: Role of aluminum during formation. *J. Mater. Chem. A* **31**, 8813 (2013).
21. G. Rani and P.D. Sahare: Effect of phase transitions on thermoluminescence characteristics of nanocrystalline alumina. *Nucl. Instrum. Methods Phys. Res., Sect. B* **311**, 71 (2013).
22. R. Bottcher, H.T. Langhammer, T. Muller, and H.P. Abicht: Evaluation of lattice site and valence of manganese in hexagonal $BaTiO_3$ by electron paramagnetic resonance. *J Phys. Condens. Matter* **17**, 4925 (2005).
23. A. Sengupta, R.M. Kadam, B. Rajeswari, A.R. Dhobale, Y. Babu, and S.V. Godbole: Characterization of Indian serpentine by X-ray diffraction, photoacoustic spectroscopy and electron paramagnetic resonance spectroscopy. *Appl. Clay Sci.* **50**, 305 (2010).
24. V. Singh, R.P.S. Chakradhar, J.L. Rao, and D-K. Kim: Synthesis, characterization, photoluminescence and EPR investigations of Mn doped $MgAl_2O_4$ phosphors. *J. Solid State Chem.* **180**, 2067 (2007).
25. K. Momma and F. Izumi: VESTA: A three-dimensional visualization system for electronic and structural analysis. *J. Appl. Cryst.* **41**, 653 (2008).
26. C. Calvo: Crystal structure of β-$Zn_2P_2O_7$. *Can. J. Chem.* **43**, 1147 (1965).
27. C. Calvo, J.P.V. Nest, and W.R. Datars: Luminescence and the cation coordination number in the phosphate system. *Mater. Res. Bull.* **2**, 283 (1967).

https://doi.org/10.1557/jmr.2013.325 Published online by Cambridge University Press